Granular Matter (2025) 27:49
https://doi.org/10.1007/s10035-025-01525-8

RESEARCH

Induced collective response in sheared granular faults exhibiting stick–slip

Zhuan Dai[1] · **Ke Gao**[1,2]

Received: 13 January 2025 / Accepted: 8 April 2025

Abstract
Granular gouge is commonplace in natural faults. Revealing the particle motion and rearrangement inside the granular gouge during stick–slip cycles can help better understand the complex processes involved in tectonic earthquakes. Here, the microscopic kinematics and collective response of a granular gouge during the two distinctive states—stick and slip phases—are analyzed based on a numerically simulated sheared granular fault system using the combined finite-discrete element method. During stick phases, the gouge locks the fault plane like a solid, but a few tiny active particle clusters exist due to scattered local contact failures between particles. When slips occur, part of the gouge flows like a liquid, and the particles in the principal slip zone are the most chaotic. The correlation of the collective response of granular particles is weak during stick phases, and the particles barely rearrange themselves, which gives opportunities for storing potential energy in the system. However, when fault slips, the gouge particles' collective response is strongly correlated, and the stored energy is released, indicating that the particles are effectively rearranged. The rearrangement of the gouge can be explained by the stress chain structures. These stress chains facilitate the cascade of the slips, which reveals why granular gouge inhibits pre-slips. Our study shows how the granular gouge reacts and rearranges during stick–slip cycles from a microscopic viewpoint and may shed light on the dynamic nucleation process of natural earthquakes.

Keywords Sheared granular gouge · Stick–slip · Deformable plate · Gouge kinematics · Collective response · Stress chain

1 Introduction

Granular gouge is commonplace in natural faults due to the continuous grinding between fault blocks [20, 25, 60] which plays a vital role in the dynamic behavior of faults and the generation of repetitive stick–slip cycles [41]. The stick phase corresponds to the inter-seismic stage, during which fault surfaces are locked and thus elastic energy is built up. The slip phase corresponds to the slip nucleation stage, where fault surfaces are unlocked and slide with each other, and elastic energy is released drastically due to gouge failure (gouge particles unlock and collide with each other) [13]. This sequence implies that the granular gouge experiences distinctively different dynamics in these two stages. Since fault surfaces interact through gouges, understanding the microscopic kinematics of granular gouges in the inter-seismic and slip stages is crucial for unveiling the complex processes involved in tectonic earthquakes.

To mimic the dynamic behavior of natural faults, researchers have incorporated granular gouges in laboratory physical experiments, i.e., shearing simulated faults with granular gouges on a laboratory scale [10, 23, 33, 34, 37, 40, 42, 55, 58]. Currently, the existing works focus on how the normal pressure [6], shear velocity [35], fluid pressure [2], temperature [52], mineral types [36], and shear displacement [54] influence the macroscopic friction coefficient (shear/normal force) during stick–slip cycles. Researchers have not been limited to how these environmental conditions influence the stability of faults; they have also studied the effects of microstructures in granular gouges. Scuderi

✉ Ke Gao
gaok@sustech.edu.cn

[1] Department of Earth and Space Sciences, Southern University of Science and Technology, Shenzhen, Guangdong, China

[2] Guangdong Provincial Key Laboratory of Geophysical High-Resolution Imaging Technology, Southern University of Science and Technology, Shenzhen, Guangdong, China

Published online: 30 April 2025

et al. [57] showed how gouges evolve with shear strain by scanning electron microscope (SEM) imaging and found that the microstructures in gouges strongly influence fault stability. Daniels and Hayman [22] sheared photo-elastic particles and showed the differences in force chains before and after slip events. They concluded that the force chain structure plays a key role in the shear zone deformation. Xing et al. [64] carried out X-ray tomography on sheared granular materials and found that the microscopic contact forces and the topology of particles are closely related to the macroscopic shear stress. The preponderance of the evidence implies that the evolution in granular gouge is closely related to stick–slip cycles. However, SEM imaging requires sample slicing, photo elastic particles are limited in 2D models, and X-ray tomography has limited resolutions to capture detailed kinematics in the gouge during slip phases. There are still mysteries about the microscopic rearrangement mechanisms inside the granular gouge during stick–slip cycles.

With the improvement of computational power in recent years, numerical simulations of laboratory earthquakes were performed for detailed granular motion that cannot be directly monitored due to the physical limitations of experimental equipment [14, 21, 24, 28, 46, 47, 62]. Concepts have been proposed to depict the microscopic evolution in granular gouge/material, including nonaffine displacement [19], granular temperature [69], slipping contact ratio [26], and topology of Delaunay tessellation [15]. Researchers not only focus on studying particles in stable sliding [69] or jamming states [68], but also pay attention to the gouge during stick–slip cycles. In addition to the precursor [26] or trigger [27] of slip events, the micro rearrangement mechanism during stick-slips is also studied. Aharonov and Sparks [3–5] simulated sheared circular granular gouges under different conditions (normal stresses, shear velocity, and gouge thickness) using discrete element method (DEM). They demonstrated how these conditions influence the shear localization and slip-modes, and corresponding contact force network evolution in the gouge is also explored. Researchers also used breakable spherical gouge grains in their numerical simulations to show how grain sizes evolve with shearing and its effects on the macro properties of faults [1, 38]. With the improvement of numerical simulation methods, fine and high-resolution microscopic data of granular particles in a more realistic numerical model are readily attainable, providing an effective tool to probe further into the microscopic kinematics and rearrangement of granular gouges during stick–slip cycles.

However, the existing works mainly adopt rigid shear plates in the numerical models, and the deformation of shear plates of granular fault systems should be considered in some large-scale faults [28]. In the laboratory, to construct large-scale sheared faults, there is research on sheared meter-scale rock faults [43, 65, 66], and some used photo-elastic materials that are much softer but can reflect a relatively large-scale behavior in a smaller size [32, 63]. These experiments are valuable references for conducting numerical simulations of microscopic granular information in large-scale granular faults. The existence of granular gouges between fault planes significantly influences the shearing behavior of large-scale faults. For example, Buijze et al. [11] found that pre-slips of plates before slip events are inhibited by the granular gouge when large-scale faults are sheared in the laboratory. Thus, relevant simulations of large-scale sheared granular faults may enable us to explain the effects caused by the granular gouge from the perspective of microscopic particle motion. Fortunately, a recently developed numerical method—the combined finite-discrete element method (FDEM) [48]—which merges finite element-based analysis of continua with discrete element based transient dynamics, contact detection, and contact interaction solutions of discontinua, provides a natural solution to modeling a large-scale fault [29].

In fact, during the stick–slip cycles, the particle mass rearranges itself through a self-organized process [7]. Specifically, external perturbation influences some particles; then, the influenced particles interact with their neighbors; finally, the perturbation may pass through the whole granular mass or disappear due to the dissipation of strain energy or weak interaction between particles. The process of how a group reacts to environmental perturbations is called collective response [8, 16–18]. The collective response in sheared granular gouges of large-scale faults during stick–slip cycles needs further exploration. Numerical simulation is an efficient way to unveil the relevant microscopic kinematics of a granular gouge. A deep understanding of the collective response of sheared granular gouge may also enable us to explain how the granular gouge influences the friction property of a fault.

Here we show that the dynamic nucleation process of fault slip depends in part on how granular gouge reacts and rearranges during the stick stage of stick–slip cycles. We analyze granular gouge during the stick–slip cycles in a simulated granular fault system using FDEM. The microscopic kinematics and collective response of the gouge in the stick and slip phases are depicted, and the accumulation and drop of the macroscopic friction coefficient are connected to explore the microscopic mechanisms in the gouge. The collective response of different states (e.g., large slip, small slip and stick phases) are compared. We connect the microscopic collective response of granular gouge with macroscopic fault states. Finally, to explain why the gouge is in distinctive states in the stick and slip phases, we show how the stress chain structure evolves.

2 Methods

In this section, we first introduce the FDEM numerical tool and the setup of the sheared fault model containing a granular gouge. Then, the method used to measure the correlation of collective response in the granular system is illustrated.

2.1 FDEM and model setup

The FDEM was originally developed by Munjiza in the early 1990s to simulate the transition of solid materials from continuum to discontinuum and the interaction between discrete solid bodies [48]. In FDEM, the finite element method (FEM) module is responsible for solving the deformation of continuum objects. Through contact detection and contact interaction processing in the discrete element method (DEM) module, complex interactions between discrete continuum objects can be captured in detail. The FDEM inherits the advantages of both FEM and DEM. When simulating the granular fault system, it can cooperate with deformable plates to sheared gouge, producing distinctive stick–slip cycles and obtaining detailed stress evolution inside the gouge. An introduction to FDEM can be found in our previous works [29–31].

We use FDEM to simulate a 2D sheared fault system with a granular gouge [29] based on an earlier photoelastic experiment conducted by Geller et al. [32]. Bi-disperse diameters (1.2 or 1.6 mm) for the nearly circular gouge particles are adopted to avoid crystallization during shear [61]. Each particle is further meshed into 24 nearly equal-sized triangle finite elements to capture its deformation. The gouge is sandwiched between two identical deformable plates (Fig. 1). A constant shear velocity (V=0.5 mm/s, in the x direction) is applied to the top stiff bar to shear the fault system, while a normal load (P=28 kPa, in the y direction) is maintained on the bottom stiff bar. The top stiff bar can only move in the x direction and the bottom stiff bar can only move in the y direction. The length of the gouge is

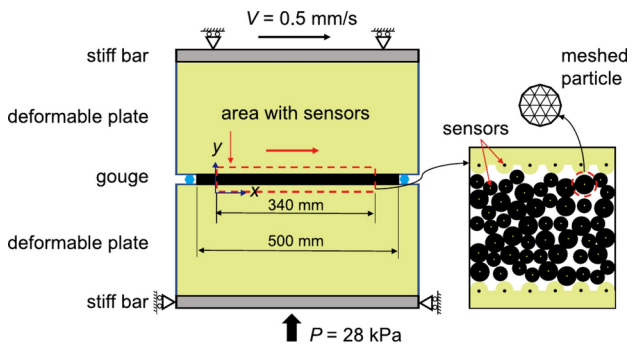

Fig. 1 Model setup. The gouge is sandwiched between two identical deformable plates. Each particle is further meshed into 24 triangle elements. There are 1917 particles with sensors, and another 143 sensors are placed on each of the top and bottom plates close to the gouge

500 mm, and the thickness is about 11 mm after consolidation. The plate boundary has semicircle "teeth" with a diameter of 1.6 mm to facilitate shear on the gouge. We place a series of "*sensors*" in the middle part of the model (red dashed rectangle area in Fig. 1) at the center of teeth and particles to monitor the particle and plate boundary motions. The displacement, velocity, and stress tensor data at each sensor point are collected every 1 ms. There are a total of 1917 particles with sensors, and 143 sensors on each of the top and bottom plates. Parameters of the model are listed in Table S1 of the Supplementary Material.

Before entering regular stick–slip cycles, the numerical model undergoes a consolidation and pre-shear stage. The shear begins when the system settles (the kinetic energy of the system is stabilized near zero). The inertial number of the model is $I = \dot{\gamma} d/\sqrt{P/\rho} \approx 2.84 \times 10^{-7} < 10^{-3}$, indicating the system is in a quasi-static shearing state, where $\dot{\gamma}$ is the shear rate, d is the particle's average diameter, P is normal pressure, and ρ is the particle's density. The $\dot{\gamma}$ is calculated by

$$\dot{\gamma} = \frac{V}{H_m}, \tag{1}$$

where H_m is the height of the model (~500 mm). The simulated results have been calibrated in our previous work, with the generated slip event magnitudes adequately following the Gutenberg-Richter distribution [29].

2.2 Characterization of collective response

The concept of collective response has been used to depict the underlying coordination mechanisms of animal groups (e.g., bird flocks, fish schools, mammal herds) [16, 51], and the concept can be applied to particles in fault gouge. Collective response is a powerful way to characterize how an animal group reacts to the perturbations of environment. The collective response is defined based on the decentralized velocity (or its magnitude) of individuals in a group, representing each individual's contribution to the response of the whole group to accommodate the perturbation from the outer environment.

Before providing a definition of collective response for the granular gouge under stick–slip cycles, we introduce a measure of the global order of a granular system, i.e., the polarization [16]

$$\Phi = \left| \frac{1}{N} \sum_{i=1}^{N} \frac{\mathbf{v}_i}{|\mathbf{v}_i|} \right|, \tag{2}$$

where $\mathbf{v}_i$ is the velocity vector of particle i, N is the total number of particles considered, and $|\cdot|$ denotes the magnitude of the velocity vector. The range of Φ is [0, 1], where $\Phi=0$ means that the velocity orientations of the particles considered are purely randomly distributed with no preference; the non-zero Φ denotes a net motion of the mass center of the entire granular system. Φ is therefore can be used as a standard measure of the global order of a granular system.

To define the collective response of a granular system, we need first to quantify the fluctuation of each particle in terms of its velocity, i.e.,

$$\mathbf{u}_i = \mathbf{v}_i - \frac{1}{N}\sum_{k=1}^{N}\mathbf{v}_k. \tag{3}$$

The fluctuation is essentially a particle's velocity deducting the velocity of the group's mass center, i.e., decentralized particle velocity relative to the whole granular system, reflecting the particle's rearrangement in the granular system. Note that the mean fluctuation of all particles is zero, i.e.,

$$\frac{1}{N}\sum_{i=1}^{N}\mathbf{u}_i = 0. \tag{4}$$

Based on this, a correlation function of the fluctuations of all particles can be defined as

$$C_{\mathrm{ori}}(r) = \frac{1}{c_0}\frac{\sum_{ij}\mathbf{u}_i\cdot\mathbf{u}_j\delta(r-r_{ij})}{\sum_{ij}\delta(r-r_{ij})}, \tag{5}$$

where $\delta(r-r_{ij})$ is a smoothed Dirac function of selecting pairs of particles at mutual distance r, and r_{ij} is the distance between two particles i and j. If the mutual distance between two particles i and j is the prescribed r, their inner product $\mathbf{u}_i\cdot\mathbf{u}_j$ contributes the most to the correlation $C_{\mathrm{ori}}(r)$. c_0 is a normalization factor that ensures $C_{\mathrm{ori}}(r=0)=1$. $C_{\mathrm{ori}}(r)$ ranges from −1 to 1. A large value of $C_{\mathrm{ori}}(r)$ implies that the fluctuations of all particles are nearly parallel (pointing in the same direction) and thus strongly correlated at the prescribed r. Conversely, when the fluctuations are anti-parallel (pointing in the opposite directions), i.e., anti-correlated, the correlation function has a negative value. On the other hand, when the fluctuations are uncorrelated, i.e., pointing in non-parallel orientations, $C_{\mathrm{ori}}(r)$ is close to zero.

The above definition essentially provides a correlation function of particles' velocity orientations (C_{ori}). Similarly, the correlation function of particles' velocity magnitudes can also be defined, i.e.,

$$C_{\mathrm{mag}}(r) = \frac{1}{c_0}\frac{\sum_{ij}\varphi_i\varphi_j\delta(r-r_{ij})}{\sum_{ij}\delta(r-r_{ij})}, \tag{6}$$

where φ is the fluctuation of a particle's velocity magnitude, i.e.,

$$\varphi_i = |\mathbf{v}_i| - \frac{1}{N}\sum_{k=1}^{N}|\mathbf{v}_k|. \tag{7}$$

The scalar fluctuation φ_i is the velocity magnitude of particle i deducting the global mean, i.e., the magnitude relative to that of the mass center, representing the scalar rearrangement of the system. Likewise, the mean of the scalar fluctuations is zero, i.e.,

$$\frac{1}{N}\sum_{i=1}^{N}\varphi_i = 0, \tag{8}$$

since there is no net velocity magnitude relative to the group's mass center. Like $C_{\mathrm{ori}}(r)$, a large positive value of $C_{\mathrm{mag}}(r)$ implies that the scalar fluctuations tend to have the same sign (either positive or negative), thus strongly correlated at the prescribed r. Conversely, when the $C_{\mathrm{mag}}(r)$ is negative, the sign of the scalar fluctuations is opposite at the prescribed r and is therefore anti-correlated. On the other hand, when the fluctuations are uncorrelated, the sign of scalar fluctuations is random, and the $C_{\mathrm{mag}}(r)$ is close to zero.

Typical shapes of correlation functions C_{ori} (or C_{mag}) are presented in Fig. 2, where the plus ("+") and minus ("–") symbols indicate the opposite orientations of velocity fluctuation or the opposite signs of velocity magnitude fluctuation, and the size of the symbol represents the fluctuation size. It is worth noting that since the fluctuation is a decentralized characterization of velocity orientation or magnitude, there must be both positive and negative fluctuation representations; thus, their summation must be zero (see Eqs. 4 and 8). When the positive and negative orientations (or magnitudes) of particles cluster in two distinct domains (e.g., Fig. 2a), the system has the strongest correlation; the correlation function traverses zero with increasing r and has a distinctive anti-correlated domain when r is greater than a certain value. If three distinct domains exist (e.g., Fig. 2b), the correlation function will traverse zero twice. For more such distinct clustering domains, more zero points of the correlation function can be observed. When the orientations (or magnitudes) of particle velocities are randomly distributed in space, i.e., with many more distinct domains, the correlation function quickly drops to ~0 with the increasing

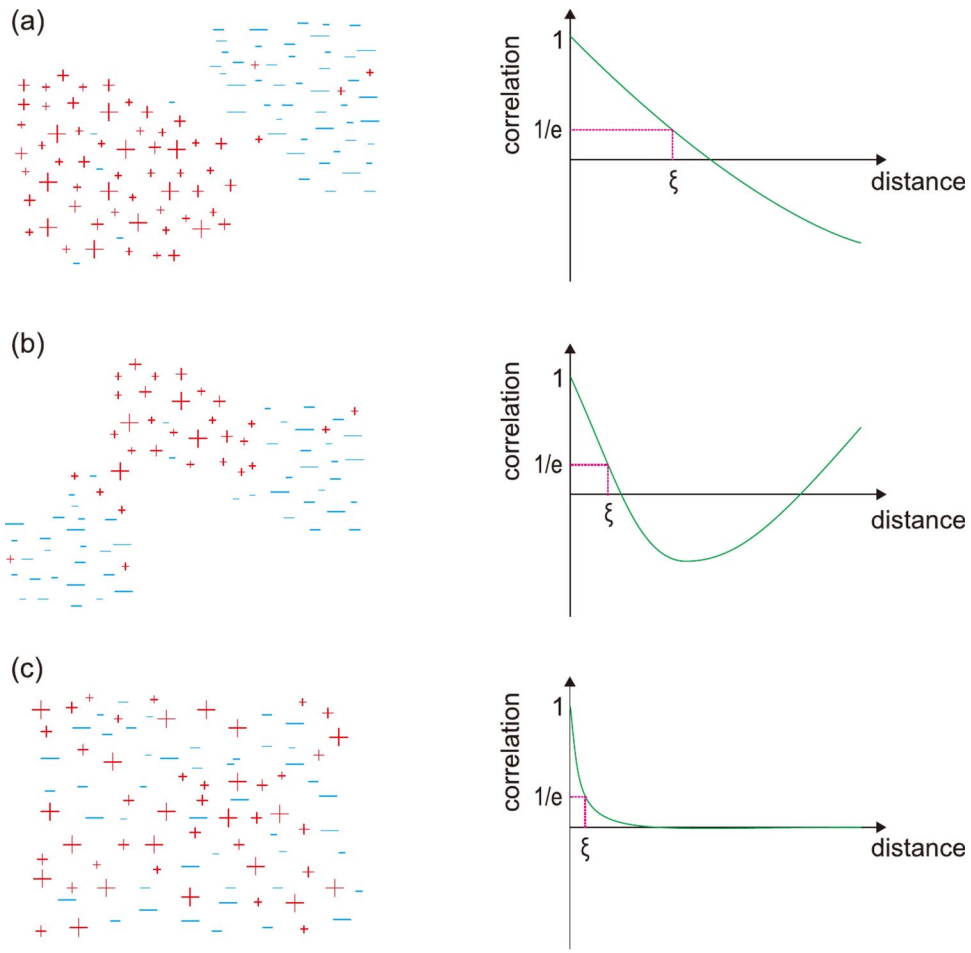

Fig. 2 Typical types of correlation curves. The plus ("+") and minus ("−") symbols indicate opposite orientations of velocity fluctuation or the opposite signs of velocity magnitude fluctuation. **a** When the positive and negative symbols cluster in two distinct domains, the correlation function traverses zero and has a distinctive anti-correlated domain after r reaches a certain value. **b** For a model with three distinct positive or negative domains, the correlation function traverses zero twice. **c** When the orientations (or magnitudes) are randomly distributed in space, the correlation function plunges to and stays around 0

r (e.g., Fig. 2c). The curve of the correlation function reflects the distribution of fluctuation in a granular gouge.

To further quantify the correlation of collective response in a granular fault system, a characteristic correlation length (ξ) is defined as the value of r when the correlation function first declines to 1/e [69]. When the positive and negative fluctuation symbols cluster in two distinct domains (e.g., Fig. 2a), the correlation of collective response is the strongest and has the largest ξ. On the contrary, when the positive and negative values are randomly distributed (Fig. 2c), the correlation is the weakest, yielding the smallest ξ. Therefore, a larger ξ indicates a stronger correlation of collective response in a granular system and vice versa.

3 Results

In this section, we first depict the general kinematics of the whole system. Then, the granular rearrangement and collective response in the gouge in both the stick and slip phases are analyzed.

3.1 General kinematics of the gouge

After 8000 ms, the fault system enters regular stick–slip cycles (Fig. 3a). Here, we define the macroscopic friction coefficient (μ), i.e., the ratio between the shear and normal stress along the plate-gouge boundary, to reflect the stick–slip cycles (Fig. 3a). Figure 3b is an enlargement of typical stick phases and slip events (red dotted rectangle area in Fig. 3a). During the stick phases, μ increases nearly linearly with slight fluctuations, representing the inter-event period. The μ drops drastically with different magnitudes, corresponding to slip events. The x velocities of 143 sensors on each plate are averaged to quantify the plate motion during the stick–slip cycles, and we denote the average velocities of the two plates as v_{pt} and v_{pb}, where subscripts 't' and 'b' denote the top and bottom plate, respectively. Generally, the slip phase accompanies a large stress drop, and the top and bottom plates also have large slip velocities but in opposite directions. In the stick phase, v_{pt} and v_{pb} are close to half the plate shear velocity (Fig. 3c and Fig. S1). Figure S1 presents the plate motion in the stick and slip phases. The gouge particles act like solids in stick phases, locking the

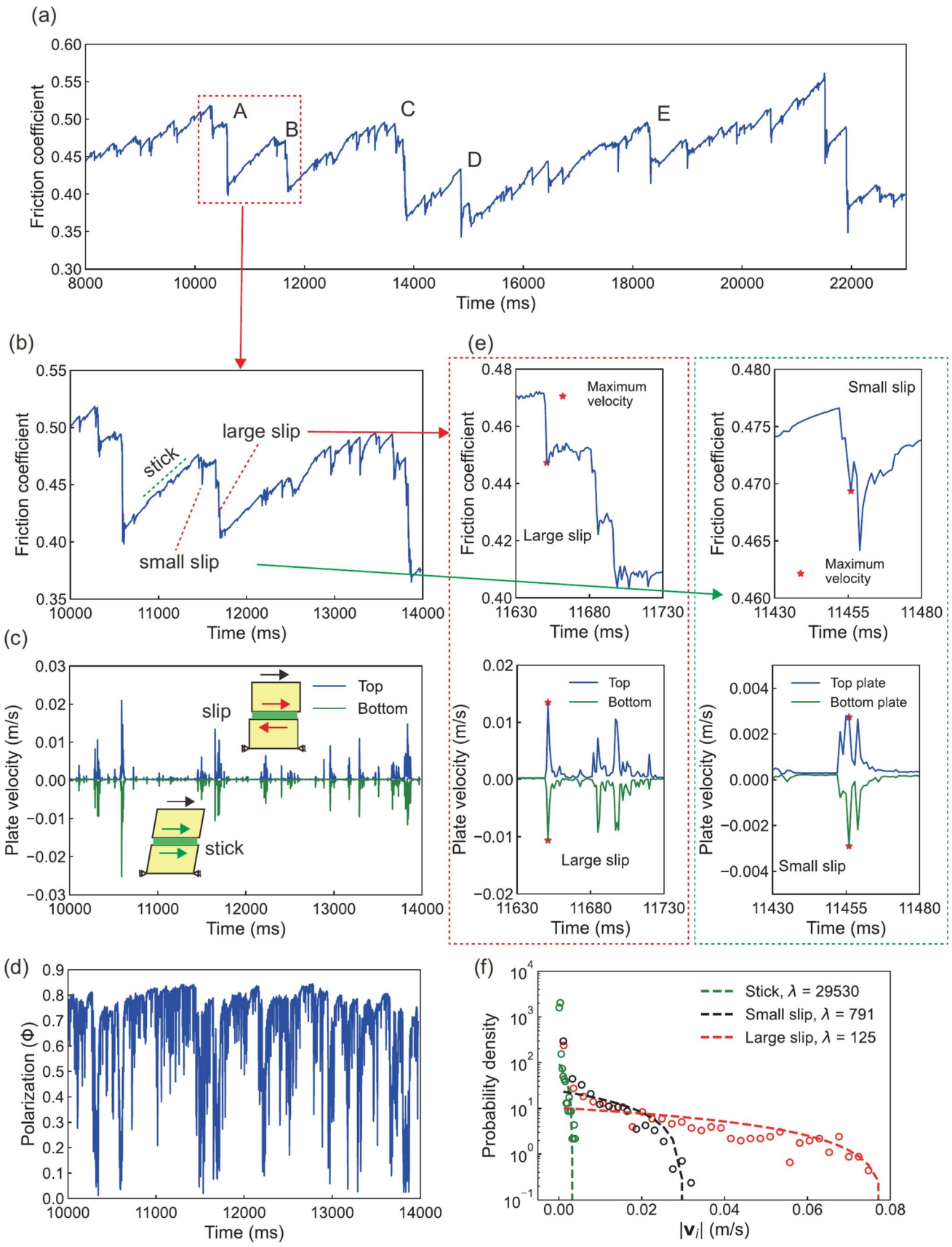
(a)
Friction coefficient
Time (ms)
A
B
C
D
E
(b)
stick
large slip
small slip
(c)
slip
stick
Top
Bottom
Plate velocity (m/s)
(d)
Polarization (Φ)
(e)
Maximum velocity
Large slip
Small slip
Top plate
Bottom plate
(f)
Stick, λ = 29530
Small slip, λ = 791
Large slip, λ = 125
Probability density
|v_i| (m/s)

Fig. 3 Overview of the model. **a** Macroscopic friction coefficient (μ) versus time. **b** Enlargements of red rectangle area in **a**. **c** Average plate velocities. **d** Polarization (Φ) of the granular gouge. **e** Plate motion of small and large slips (marked in **b**). **f** Probability densities of gouge particle velocities in three different states

top and bottom plates so they move almost together. In the slip phase, the particles move relatively freely.

The motion of the whole granular mass is depicted by polarization (Fig. 3d). In stick phases, the polarization generally has a high value (~0.8), which means the granular gouge has a strong order and tends to move in a particular orientation. However, in slip phases, the polarization drops to ~0, representing a sharp order decrease in the gouge, and the mass center oscillates. Therefore, the kinematics in the gouge are distinct in the stick and slip phases. In the three time stamps selected, respectively corresponding to the three phases marked in Fig. 3b, i.e., one in the stick phase (10,880 ms), one small slip (11,455 ms) and one large slip (11,650 ms), the probability densities of the velocity magnitudes of the gouge particles decrease nearly logarithmically (probability density fitted by $f(|\mathbf{v}_i|) = -\lambda e^{|\mathbf{v}_i|+c}$) but with distinct decline slope λ (Fig. 3f). From stick, small slip to large slip, the λ changes from 29,530,791 to 125. Correspondingly, their macroscopic behaviors also vary markedly. For example, the friction drops and the plate velocities for the small and the large slips differ in magnitude (Fig. 3e). We can also find that a slip phase contains several small friction drops, and the corresponding plate velocities have different spikes in each slip event.

In the following sections, we demonstrate the collective response and its correlation in different states. Here, we define a series of large slip events with the maximum plate velocity magnitude ($|v_{pt}|$ or $|v_{pb}|$) larger than 10^{-2} m/s. Examples of them are marked in Fig. 3a from A to E. The plate velocities at these slips are shown in Fig. S2. We denote the moment with the largest plate velocity as the "mainshock", the slip events before as "foreshocks", and the ones after as "aftershocks". In these series of major slip events, there are sometimes "calm periods" between foreshocks, mainshocks, and/or aftershocks, but with a plate velocity obviously higher than that in the stick phases. Similarly, we define a series of small slip events with maximum $|v_{pt}|$ or $|v_{pb}|$ larger than 10^{-3} m/s but smaller than 10^{-2} m/s. The period with no clearly distinguishable slip event but a linearly increasing μ is defined as stick phases (maximum $|v_{pt}|$ or $|v_{pb}|$ smaller than 10^{-3} m/s). We set these thresholds to ensure that the large slip events correspond to the obvious large stress drops (e.g., A–E in Fig. 3a), small slip events correspond to much smaller stress drops, and the stick phase corresponds to the state where shear stress can be built up.

3.2 Collective response during stick–slip cycles

Here, using the three phases marked in Fig. 3b as an example, i.e., a stick phase, a small slip, and a large slip, we study the collective response of the granular gouge in a stick–slip cycle. Since in the stick phase, the particle motion at each time stamp is similar (as demonstrated in Fig. S3), we only select one time stamp (time = 10,880 ms) as a typical representative. For the small and large slips, we respectively select two time stamps with the maximum local plate velocities, i.e., the small slip at 11,455 ms and the large slip at 11,650 ms, representing the main shock of these two slip events (marked in Fig. 3e with a red star). We also examine the whole slip phase in this stick–slip cycle (Videos S1, S2), and find that the slip events have similar granular particle motion characteristics. The three time stamps we have selected can reasonably reflect the kinematics of the granular gouge during stick–slip cycles.

Firstly, we focus on the velocities of gouge particles. In the stick phase, most particles move in a certain direction (Fig. 4a). However, particles that are distinctively more active than others still exist. Therefore, we infer that although the gouge acts like a solid during the stick phases, not all particles are locked; some still vibrate and collide, evidencing the non-smooth increase of μ in the stick phase. In the slip phase, both the small and large slips have distinct domains of high and low-velocity particles (Fig. 4b, c). The particles in high-velocity domains are rearranging, and there are more high-velocity particles in the large slip. In high-velocity domains, particles are moving in different directions. Clear boundaries between clusters with different moving directions can be observed (See Fig. S4e and h), meaning these clusters collide and shear with each other. Notably, in the large slip (Fig. 4c), the sizes of high-velocity domains are larger than those in the small slip (Fig. 4b), and there are more such clusters, indicating a more drastic rearrangement in large slips.

Then, we use the decentralized particle velocity, i.e., the fluctuation $\mathbf{u}_i$, to demonstrate how particles move relative to the gouge's mass center. In the stick phase, most particles are locked and barely move relative to each other (Fig. 5a). However, a few particles with large magnitudes of fluctuation tend to appear in pairs with opposite moving orientations. We infer that this is caused by the sudden contact failure due to rolling (space expansion makes particles roll with each other) or sliding (shear force between particles exceeds the friction limit) [69]. Although the granular gouge has a strong order in the stick phase (i.e., large polarization Φ and the gouge's mass center moves towards a specific direction), the collective response is weak in this stage because most particles are confined by their neighbors and cannot rearrange freely. However, in the slip phase, parts of

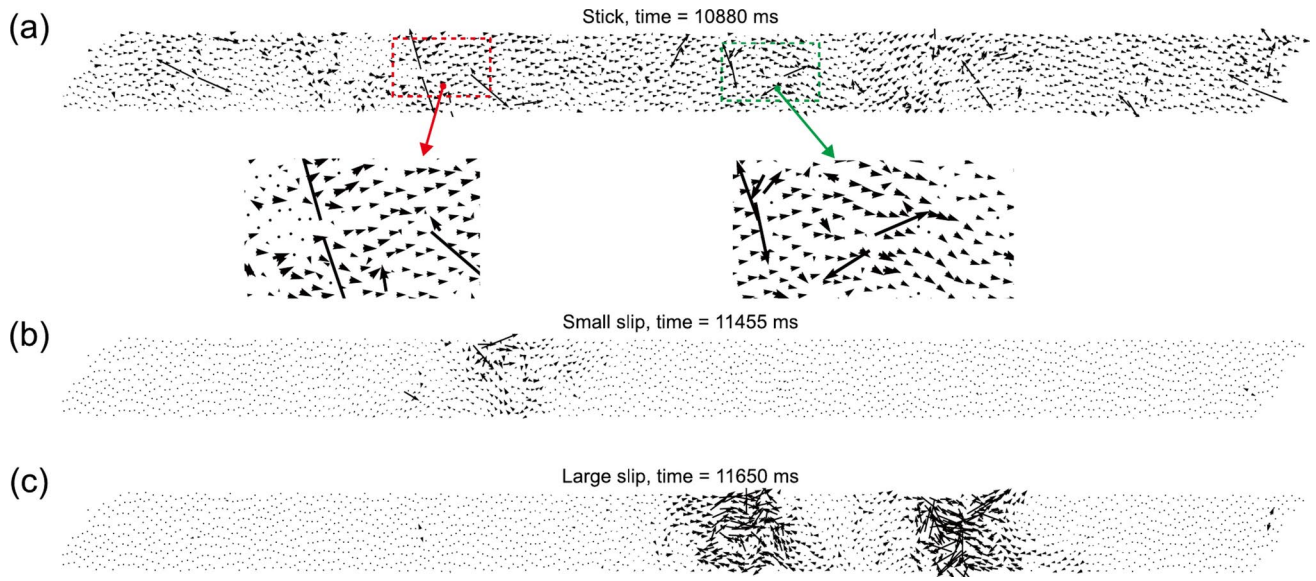

Fig. 4 Particles' velocity vectors. **a** Stick phase. **b** Small slip. **c** Large slip. See Fig. S4 for a cloud map of the velocity field

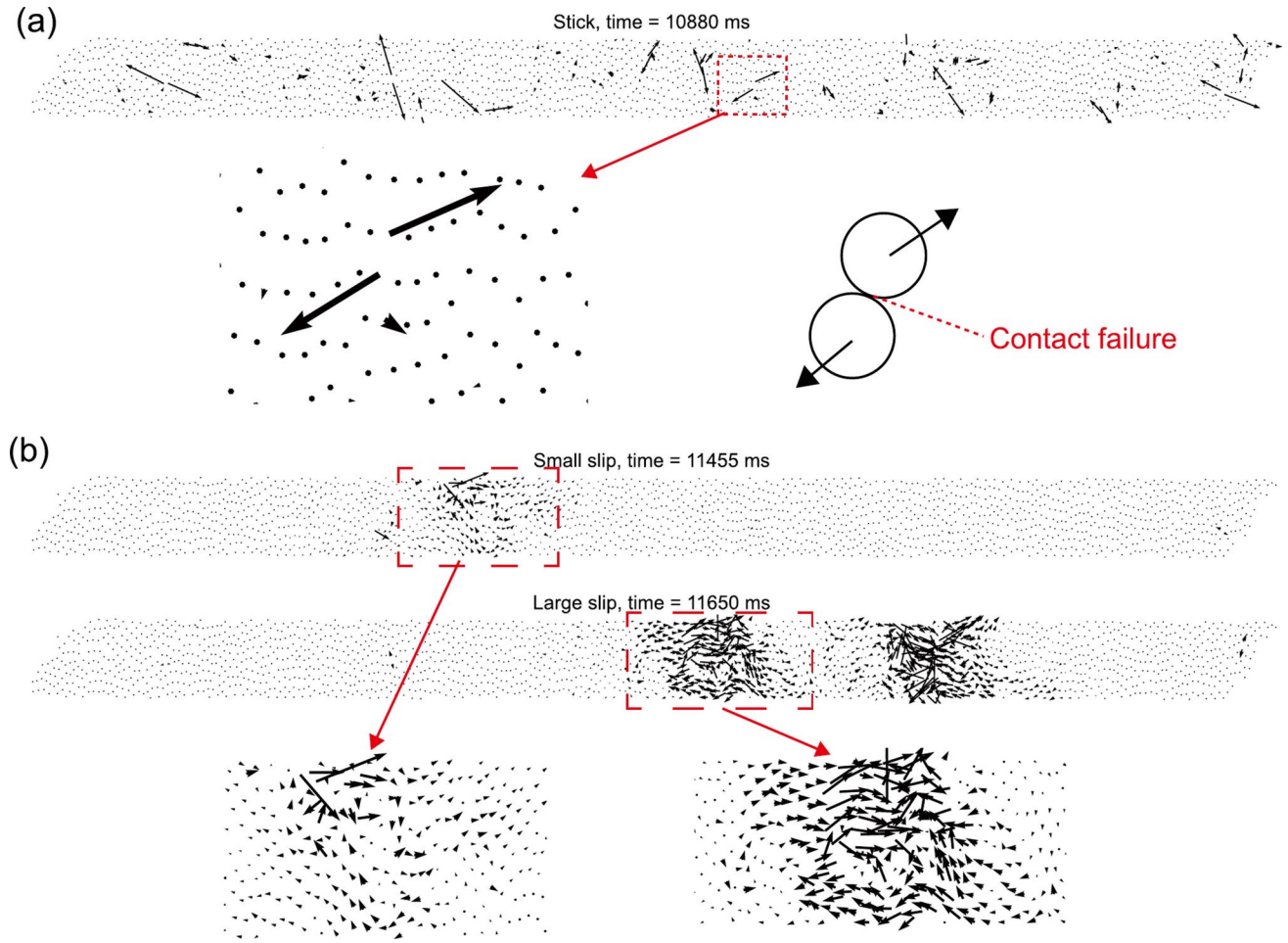

Fig. 5 Particle fluctuation vectors and the background mechanism. **a** Quiver plot of fluctuation $\mathbf{u}_i$ in stick phase; active particles exist due to scattered contact failure. **b** Quiver plot of fluctuation $\mathbf{u}_i$ in slip phases; some particles flow like a fluid.

the gouge particles flow like fluid and rearrange efficiently (Fig. 5b). The granular mass has a weak global order (i.e., low polarization Φ) in the slip phase, but we notice a strong correlation of collective response. Because the particles start to flow, particles with similar velocity orientations tend to cluster together.

To demonstrate the particles' rearrangement, we explore the relationship between the particles spatial positions and velocities in the two extreme time stamps selected earlier, i.e., the stick (time = 10,880 ms) and the large slip (time = 11,650 ms) time stamps. In our simulated granular fault, the particle velocities in the x direction (the shearing direction) are more closely related to their rearrangement (the motion in the x direction is more intense than that in the y direction). Here, to facilitate visualization and comparison, the x velocities (v_{xi}) and displacements (d_{xi}) of each particle are plotted by projecting these values to the x and y axes according to their spatial positions (Fig. 6). The left panel of Fig. 6 presents the results in the stick phase, while the right panel shows the results in the large slip.

The particles with high velocities (v_{xi}) are rare in the stick phase (Fig. 6a, b). However, in the large slip, high-velocity particles are clustered in places where the failures occur (Fig. 6f). Particles near the plate move toward a certain direction because of the driving of the plates (Fig. 6g). After a full stick phase (marked in Fig. 3b, from 10,780 to 11,380 ms), all particles move to a certain orientation, and we observe a linear increasing trend in the y direction (Fig. 6c, positive d_{xi}). On the other hand, after a full large slip (marked in Fig. 3b, from 11,630 to 11,730 ms), the particles near the top and bottom plate move in reverse directions (Fig. 6h).

The average v_{xi} fluctuates in the y direction in the stick phase (Fig. 6d). Meanwhile, the average $|\mathbf{v}_i|$ has a higher value in places with a certain distance to the plates (Fig. 6e), indicating that these places are more active and more contact failures occur here due to less confinement by the plates. On the contrary, in the large slip, the shear localization zone does exist when a slip occurs (Fig. 6i). The $|\mathbf{v}_i|$ at the main shock has a similar average value in the direction perpendicular to the fault (Fig. 6j). However, the average v_{xi} has a zero point (Fig. 6i), meaning that in the shear localization zone the v_{xi} has different directions; therefore, the particle collides and fractionates fiercely with each other. This spatiotemporal localization of energy dissipation may explain why the gouge in the principal slip zone is finer than the surrounding areas in real experiments [54].

3.3 Correlation length during stick–slip cycles

The correlation functions C_{ori} and C_{mag} in the stick phase and in the small and large slips mentioned in Sect. 3.1 are respectively shown in the three rows in Fig. 7. In the stick phase, C_{ori} quickly drops to zero with increasing r and then fluctuates slightly (Fig. 7a), reflecting that particle locking weakens the correlation of particles' velocity orientation. However, C_{mag} in the stick phase has more violent fluctuations, indicating that the failure of contacts renders a higher velocity for their neighboring particles (Fig. 7b). Nevertheless, the fluctuations are too small to trigger large-area particle flow (Fig. 7b). With the increasing r, the C_{ori} of the small slip has an anti-correlation domain before stabilizing around zero (Fig. 7c), which differs from C_{ori} in the stick phase (Fig. 7a). Therefore, when slips occur, particle mass does have a stronger correlation of collective response. The C_{ori} of the large slip goes through a more correlated-anti-correlated traverse (Fig. 7e) due to more support structure failure and particle rearrangement in several locations. The shapes of C_{mag} are similar in both the small and large slips (Fig. 7d, f), resembling Fig. 2b. This can be explained by the conversion from strain energy to kinetic energy during the failure. Particles closer to failure have higher velocity magnitudes. Notably, the single domain for high-speed particles (similar to Fig. 2b) tells us that despite several support structure failures, they may originate from the same small contact failure.

In addition to the three typical time stamps analyzed above, we also extract the results from more time stamps and calculate the statistics of the correlation lengths (ξ, see Sect. 2.2) of the granular gouge in the stick, small and large slip phases to quantify and compare the correlations (Fig. 8a, b). The average ξ_{ori} in these three phases are similar (Fig. 8a); however, we notice that the C_{ori} in slip phases fluctuate around zero before stabilizing around zero (Fig. 7c, e), telling us the gouge system traverses from correlated to anti-correlated. Then, we calculate the correlation strength (C_{st}, integral of the absolute value of the correlation function) in these three phases to check the fluctuation of C_{ori} (inset of Fig. 8a), and find that the C_{st} in the stick phase is less than that of the small and large slip. The ξ_{mag} has low values in the stick phase, representing a weak collective response. The ξ_{ori} and ξ_{mag} in the small slip have a remarkable fluctuation range, possibly due to the more random failure positions. We find no distinct difference of ξ in the foreshock, main shock, and aftershock, which indicates that each failure has a similar mechanism (Fig. 8c, d). Finally, we compare ξ in the stick and calm period in the large slip (Fig. 8e, f). The ξ of the calm period in the large slip has a much larger value than that in the stick phase, telling us that the particles are more active than the stick phase and are easy to fail in the calm period of the large slip.

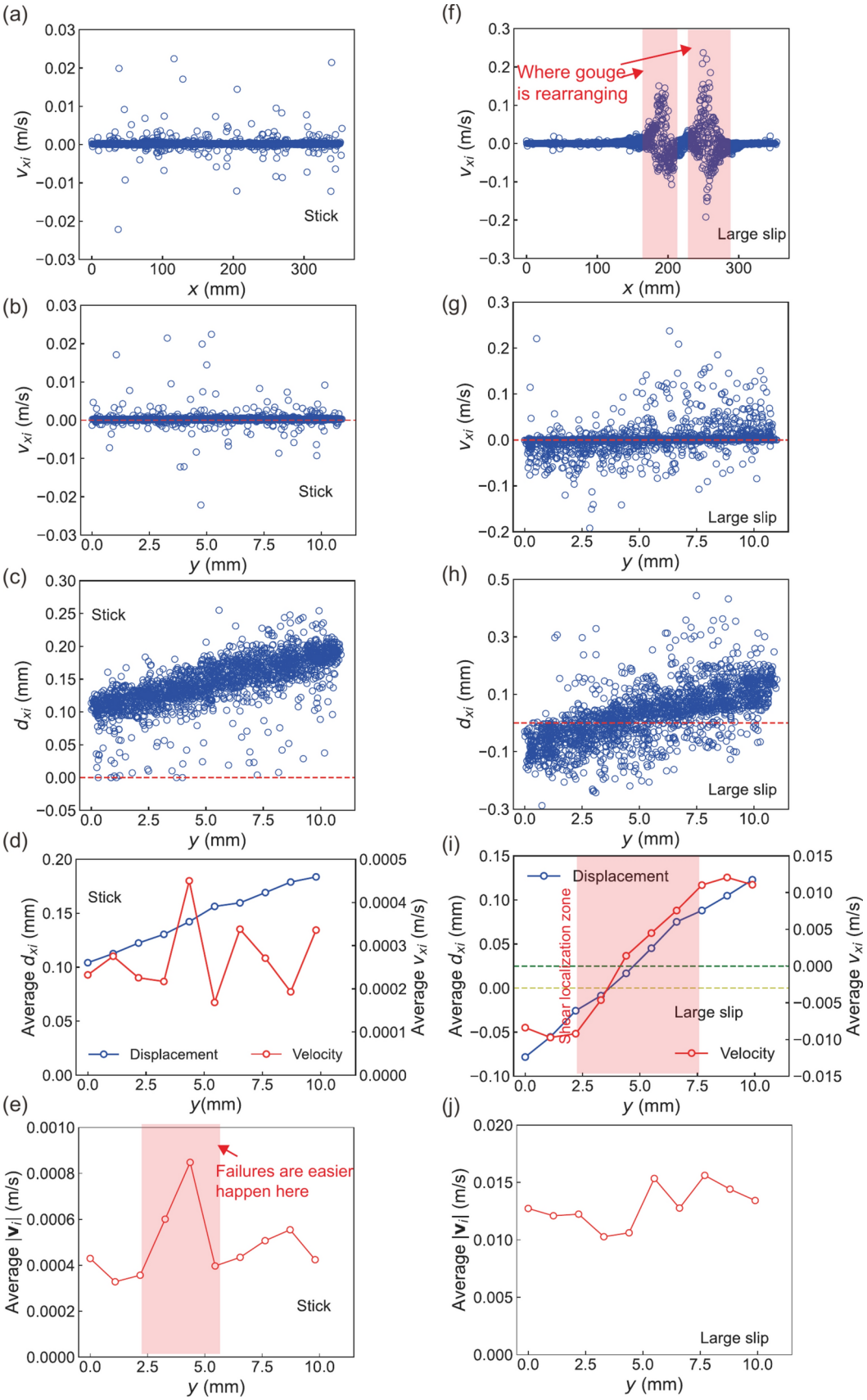
(a)
Stick
v_{xi} (m/s)
x (mm)
(b)
Stick
v_{xi} (m/s)
y (mm)
(c)
Stick
d_{xi} (mm)
y (mm)
(d)
Stick
Average d_{xi} (mm)
Average v_{xi} (m/s)
Displacement
Velocity
y(mm)
(e)
Failures are easier happen here
Stick
Average $|\mathbf{v}_i|$ (m/s)
y (mm)
(f)
Where gouge is rearranging
Large slip
v_{xi} (m/s)
x (mm)
(g)
Large slip
v_{xi} (m/s)
y (mm)
(h)
Large slip
d_{xi} (mm)
y (mm)
(i)
Displacement
Shear localization zone
Large slip
Velocity
Average d_{xi} (mm)
Average v_{xi} (m/s)
y (mm)
(j)
Large slip
Average $|\mathbf{v}_i|$ (m/s)
y (mm)

Fig. 6 Velocities and displacements of gouge particles. Left panel **a**–**e** is for the stick phase: **a** Scatter plot of particles' x velocity (v_{xi}) projected along the x axis according to their x coordinates; **b** Scatter plot of v_{xi} projected along the y axis according to their y coordinates; **c** Scatter plot of particles' x displacement (d_{xi}) projected along the y axis according to their y coordinates (10,780–11,380 ms); **d** Blue line: averaged d_{xi} at each y value; red line: averaged v_{xi} at each y value; **e** Average $|\boldsymbol{v}_i|$ at each y value. Right panel **f**–**j** is for the large slip: **f** Scatter plot of v_{xi} projected along the x axis. **g** Scatter plot of v_{xi} projected along the y axis. **h** Scatter plot of d_{xi} projected along the y axis (11,630–11,730 ms). **i** Blue line: averaged d_{xi} at each y value. Red line: averaged v_{xi} at each y value. **j** Averaged $|\boldsymbol{v}_i|$ at each y value. See Fig. S4 for cloud map of velocity field

3.4 Rearrangement mechanism of stick–slip granular gouge

The evolution of the granular gouge's collective response during stick–slip cycles may be interpreted from the viewpoint of stress chain evolution. Under the shear and normal load, the gouge particles contact each other, and the stress chain structures with strong heterogeneity are formed. The stress chain is closely related to the motion and rearrangement of the particles and may explain how the gouge particles respond to the outer environment. Here, we choose the maximum shear stress (τ_{max}) monitored at each sensor point in the gouge to present the chain-like structures (Fig. S5). We draw the particles with higher stresses and velocities for the three phases mentioned earlier (see Fig. S6 for details). The dip angles of the stress chains are roughly similar and aligned in directions that can resist the shear and normal load (Fig. 9a). High-velocity particles are evenly distributed in space in the stick phase (Fig. 9b), whereas in the slip phases, they cluster and form the stress chain structures (Fig. 9c, d).

Such a granular gouge rearrangement can be explained by the heterogeneous stress distribution in the gouge particles, i.e., the stress chain structures in the gouge. When failure occurs on a strong stress chain, the dramatic release of kinetic energy enlarges the domain of high-velocity particles (see supplementary Videos S1, S2). Then, the particle mass calms down and fails again because the unstable system yielded in the last failure renders an unstable system. We also find that the velocity orientations of high-velocity particles change dramatically. We draw a diagram in Fig. 9e to illustrate the slip mechanism. When a supporting stress chain structure fails, the particles near this failure begin to flow and tend to move with the plate they are close to (large black arrow); particles further away will flow to fill the void space (small black arrow). Then, the quakes pass through the still-locked particles, inducing another failure (cascade mechanism). The particle mass calms down after several failures and may enter a new stick cycle or fail soon.

We animate the stress chains in the stick and large slip to depict how they evolve in the stick–slip cycles. In the stick phase, only minor changes in stress chains can be found (see supplementary Video S3). Combined with the displacement of particles (Fig. 6c, d), we infer that the stress chains rotate slightly during the stick phases to support the plates, resulting in a thicker gouge and leaving more room for particles to rearrange [29]. From the motion of high-velocity particles, we find that particle rearrangement indeed occurs during the stick phase; however, no strong stress chain fails, and such failure has a minor effect on the macroscopic friction coefficient. In the slip phase (see supplementary Video S4), we observe high-velocity particles clustering around strong stress chains, indicating the dramatic rearrangement of particles along these strong stress chains. The stress chains may adjust slightly or disappear quickly and then reappear nearby. This supports the view that a slight change in strong stress chains can tremendously affect the particle system [44, 49, 50]. Therefore, large slips in the granular fault system tend to cascade (failure of one stress chain induces other stress chain failures, Fig. 9), which explains why the gouge inhibits pre-slips (slow, localized slip) before large slip events when shearing large-scale faults in the laboratory [11, 12].

4 Discussion

During the stick–slip cycles of the granular gouge, the stick phase corresponds to a weaker correlation of collective response, whereas the particle mass does reach a certain degree of correlation to rearrange itself in the large slip. When large slips happen, the granular mass has higher C_{st} (Fig. 10a, b) and ξ_{mag} (Fig. 10c, d) than the stick phase. The plate velocity in places adjacent to the gouge reflects the intensity of kinetic friction dissipation between the plates and the particles and thus the energy consumption rate. In the stick phase, such intensity of friction is low, and the correlation of collective response is weak in the gouge. This may be caused by the fact that the particles are locked by their neighbors, and they barely arrange themselves to accommodate the shear load. However, in the slip phase, the plates slip at a higher velocity, and thus the intensity of friction is high, and the correlation of collective response is strong in the gouge due to the efficient particle flow and rearrangement. The above analyses link the macro states of the granular mass and the micro collective response of particles. Specifically, in a granular gouge, the weak correlation of collective response means that the granular mass shows solid-like behavior due to individual particles confining each other; thus, the system cannot freely cope with the changes to the external environment and is capable of storing potential energy. Conversely, if the collective response of granular mass strongly correlates, the granular mass

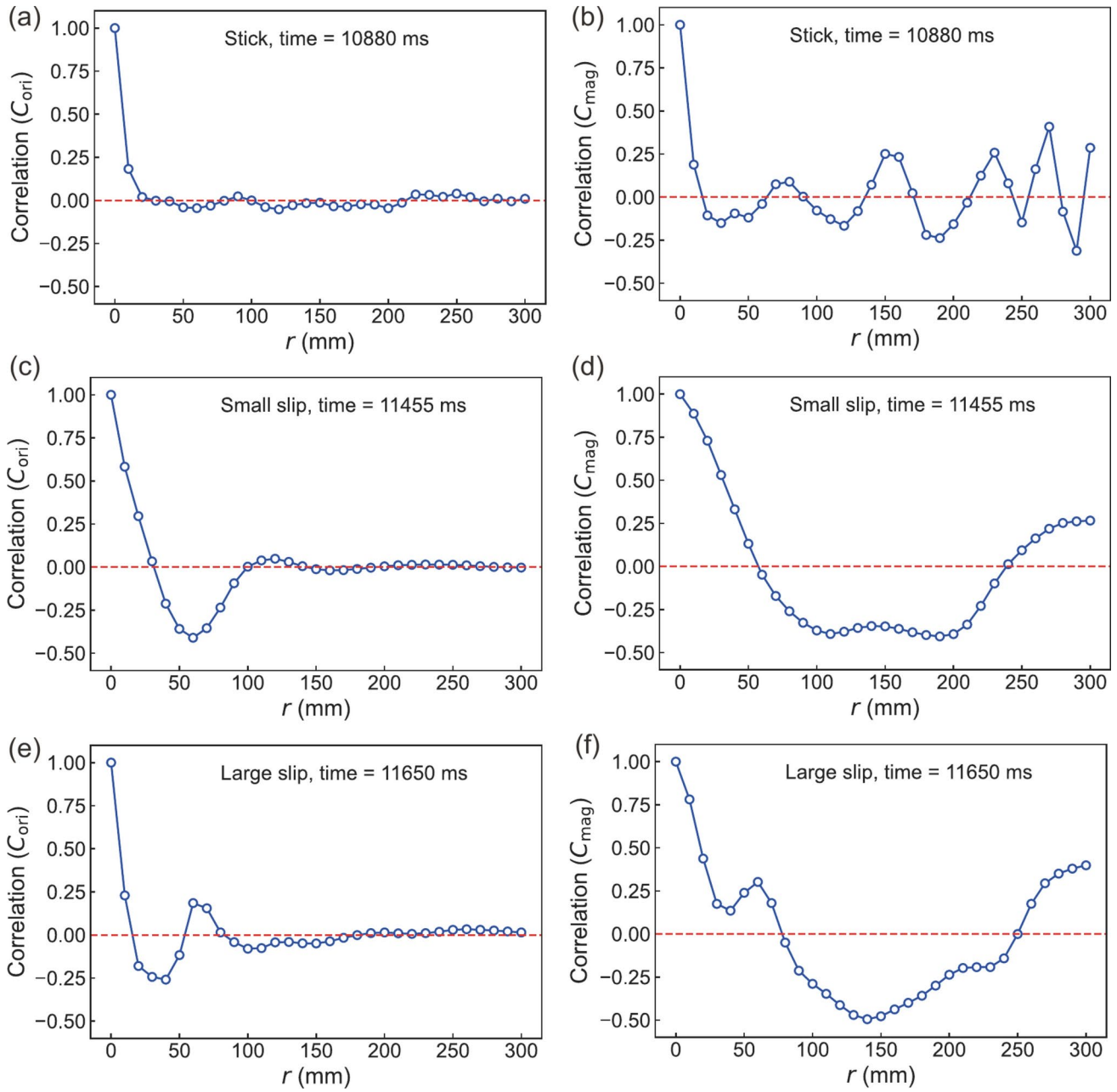

Fig. 7 Correlation functions of the gouge in the three different phases. From the top to the bottom row, they are the stick phase, the small slip and the large slip. The left column presents the correlation function of particle velocity orientation, and the right column shows the correlation function of velocity magnitudes

shows fluid-like behaviors, and the system can rearrange itself efficiently to adapt to the outer environment. Energy is consumed dramatically.

Compared to the stress states in the small-scale sheared granular faults [3–5, 39], the high-stress areas and low-stress areas in large-scale faults are more distinctly interlaced between each other (Figs. 9, S5, and S6). Correspondingly, the motion of particles is also interlaced along faults when large slips occur due to plates being deformable (Fig. 5, Fig. S4). The simulated fault here shows and explains how the granular gouge flows in and between these high-stress areas and low-stress areas (Fig. 9). We notice that all slip events in Videos S3, S4 show similar patterns. Therefore, in this kind of granular fault, the granular gouge rearrangement may have a similar mechanism as we have described before. After each slip event, the stress chains also show similar structures. The properties of the structures (interval distance, orientation) may be influenced by the normal stress, grain size distribution, particle shape, and fault roughness, which need to be further studied in the future.

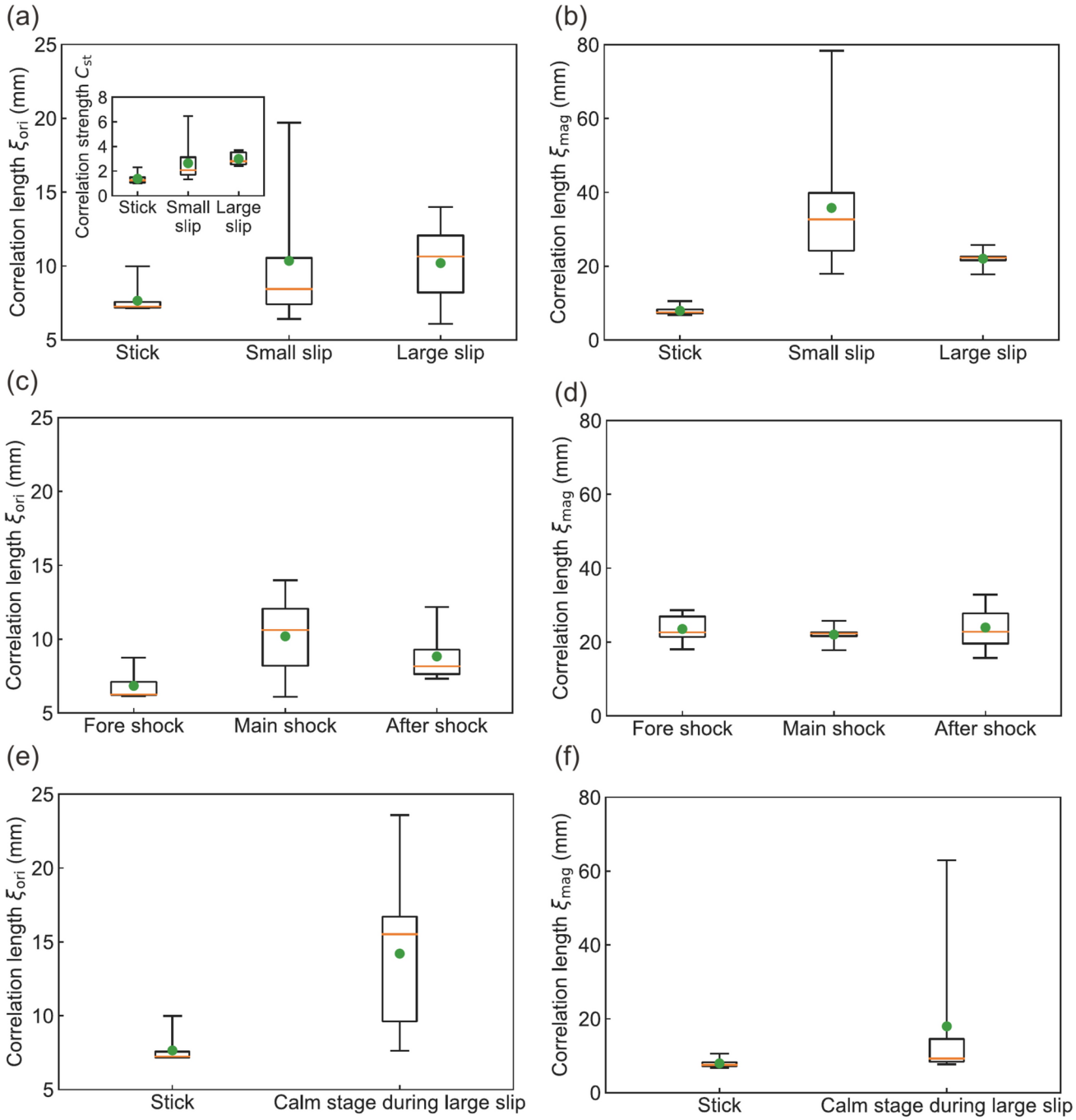

Fig. 8 Box plot of the correlation lengths in different phases. The horizon lines of the box represent 0, 25%, 50%, 75%, and 100% quantiles, respectively, from bottom to top, and the green dot represents the mean value. **a** and **b** ξ_{ori} and ξ_{mag} of the stick, small slip and large slip, respectively. Inset in **a**: Correlation strength of velocity orientation in the stick phase, small slip and large slip. **c** and **d** ξ_{ori} and ξ_{mag} of foreshock, main shock and aftershock. **e** and **f** ξ_{ori} and ξ_{mag} in the stick and calm period in the large slip

Here, compared to the slip phase, we admit that during the stick phase the collective response pattern only evolves slightly (see supplementary Video S3). Therefore, the collective response or particle velocity field may not be a perfect tool to describe the microevolution of the granular gouge during the stick phase. The deformation of the topology structure of granular mass [64] and the evolution of the stress field [67] may be more suitable indicators to describe the microevolution in the stick phase. However, this part is beyond the scope of this paper. Besides, our model is purely elastic, and the granular gouge has bi-disperse diameters. However, in natural faults, the gouge grains will be crushed during the slip phase and the size distribution of the grains shows the power-low distribution [9, 56]. Moreover, the

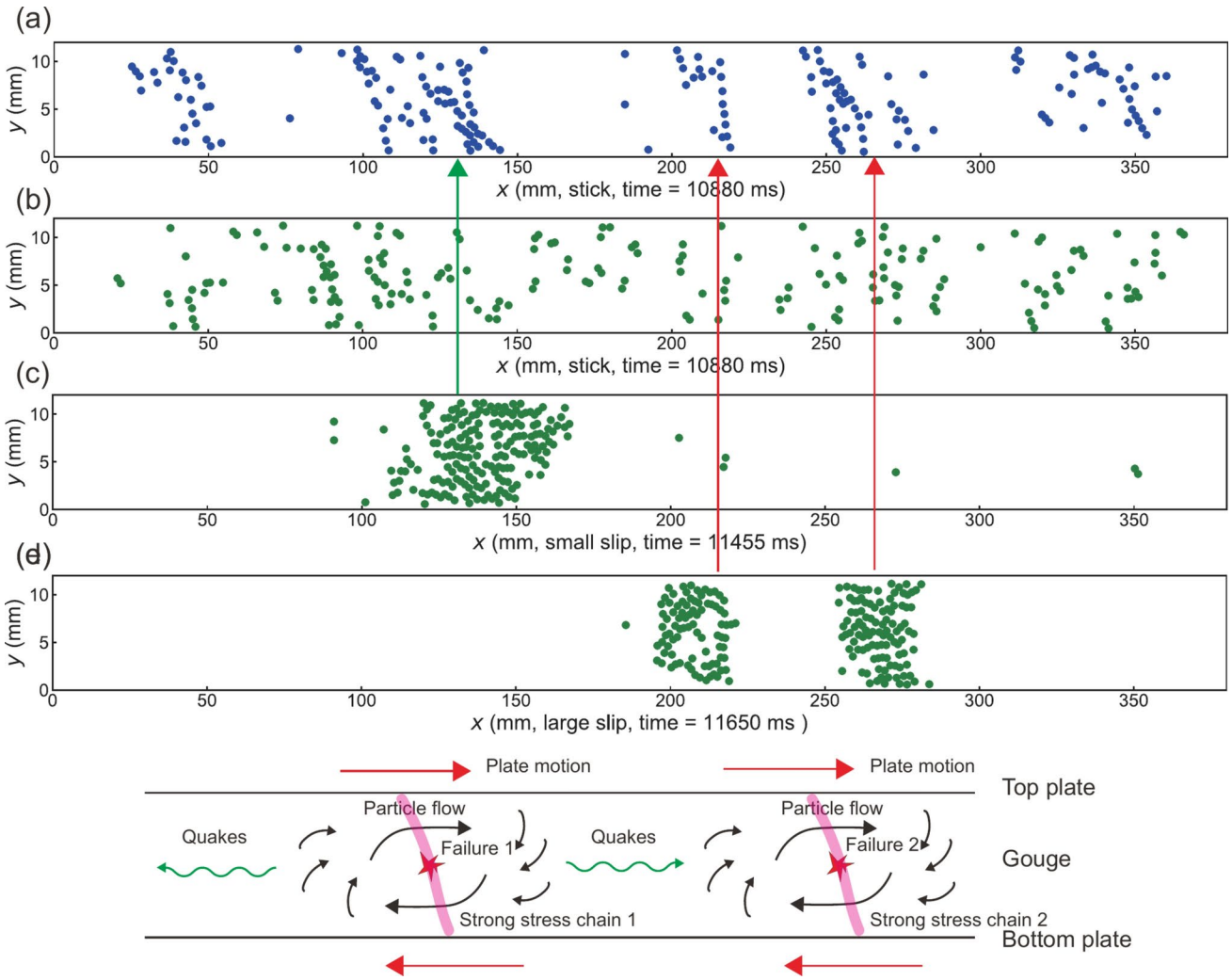

Fig. 9 Stress chains and high-velocity particles. **a** top 10% particles with the maximum τ_{max} in the stick phase, manifesting the chain-like structures. **b**–**d** are the top 10% particles with the maximum $|\mathbf{v}_i|$ in the stick, the small slip, and the large slip, respectively. **e** Mechanism of slips. When a support structure fails, the particles near this failure begin to flow and tend to move with the plate they are close to (large black arrow); particles away from the failure points flow and fill the void space (small black arrow). Then, the quakes pass through the still-locked particles and induce other failures (cascade mechanism). The particle mass calms down after a series of failures and may enter a new stick–slip cycle

complex geometry of fault planes [53, 59] and the chemical reaction of minerals in the coseismic stage can also influence the granular rearrangement [45]. Detailed studies about how grain breakage, grain size distributions, fault plane geometry, and chemical reactions influence granular rearrangement in large-scale granular faults can be conducted in the future.

5 Conclusions

We use finite element-based analysis of continua with discrete element based transient dynamics, contact detection, and contact interaction solutions (FDEM) to explore the kinematics of gouge particles in a sheared granular fault system subjected to stick–slip cycles. We show that the particle motion in the stick and slip phases have distinct characteristics. In the stick phases, the particles are locked like solids; there is no apparent shear localization but contact failure can easily occur in places with a certain distance from the plates because of less confinement. In the slip phases, some particles flow like fluid, and shear localization appears. In the principal slip zone, the motion of particles is more chaotic, indicating that the particles are colliding and frictionating. This spatiotemporal localization of energy dissipation explains why the particles in principal slip zone are smaller in real fault gouges.

Analysis of correlations of the collective response of gouge particles in the stick and slip phases shows that the granular mass has a stronger correlation in the slip phase

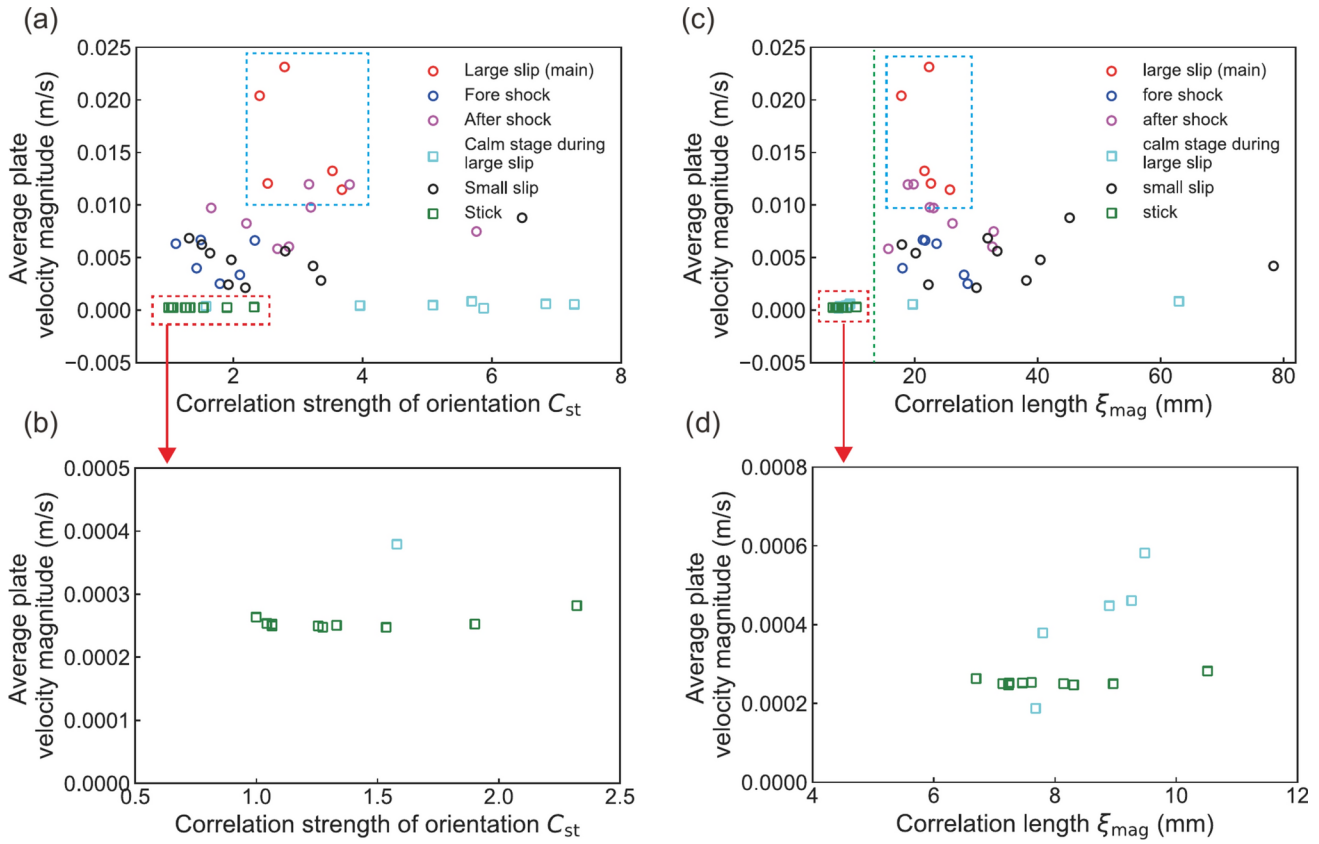

Fig. 10 Relationship between the correlation of collective response and plate velocity. **a** Scatter plot of correlation strength of particle velocity orientation versus plate velocity. **b** Enlargement of the red dashed box in **a**. **c** Scatter plot of correlation lengths of particle velocity magnitude versus plate velocity. **d** Enlargement of the red dashed box in **c**. The red dashed box shows where the stick stamps are, and the blue dashed box shows the stamps of large slips

compared to the stick phase, reflecting that the particles can rearrange efficiently in the slip phase while confined by each other in the stick phase. We link the macroscopic states of granular mass and the microscopic collective response of particles: if a granular mass has a weak correlation, the granular mass shows solid-like behavior and can store potential energy; conversely, if a granular mass has a strong correlation, it shows fluid-like behavior, and the energy is released drastically.

The granular flow distributes interlacedly along faults when large slips occur in large-scale faults. The rearrangement in granular gouge can be explained by the stress chain structures. In the granular gouge, the stress chain structure is highly heterogeneous, and the slip event is closely related to the rearrangement of particles on strong stress chains. Slight changes in a strong stress chain can cause large macroscopic friction drops, which is a finding consistent with previous inferences in the literature [44, 49, 50]. In the stick phase, the stress chain structure rotates slightly to support the plate, which leaves more space for particle arrangement. The stress chain structures cannot undergo large shear displacements before failure. Therefore, the large slips in the granular fault system tend to cascade, which explains why the gouge inhibits pre-slips before earthquakes. Our work implies that understanding the complex processes involved in earthquakes needs to account for evolving processes in the stick phase of the tectonic cycle.

Supplementary Information The online version contains supplementary material available at https://doi.org/10.1007/s10035-025-01525-8.

Acknowledgements This work is supported by the National Natural Science Foundation of China (42374070) and the Guangdong Provincial Key Laboratory of Geophysical High-resolution Imaging Technology (2022B1212010002). Zhuan Dai analyzed the data and drafted the manuscript. Ke Gao carried out the numerical simulation and revised the manuscript.

Author contribution Z. D. analyzed the data and drafted the manuscript. K. G. carried out the numerical simulation and revised the manuscript.

Data availability The codes to characterize and visualize the collective response can be found at https://github.com/xiaoDai4/Stick-slip-induced-collective-response-in-sheared-granular-fault. Data is provided within the manuscript or supplementary information files.

Declarations

Conflict of interest The authors declare no competing interests.

References

1. Abe, S., Mair, K.: Effects of gouge fragment shape on fault friction: new 3D modelling results. Geophys. Res. Lett. (2009). https://doi.org/10.1029/2009GL040684
2. Acosta, M., Passelegue, F.X., Schubnel, A., Violay, M.: Dynamic weakening during earthquakes controlled by fluid thermodynamics. Nat. Commun. **9**, 3074 (2018)
3. Aharonov, E., Sparks, D.: Rigidity phase transition in granular packings. Phys. Rev. E **60**, 6890–6896 (1999)
4. Aharonov, E., Sparks, D.: Shear profiles and localization in simulations of granular materials. Phys. Rev. E **65**, 051302 (2002)
5. Aharonov, E., Sparks, D.: Stick-slip motion in simulated granular layers. J. Geophys. Res. Solid Earth (2004). https://doi.org/10.1029/2003JB002597
6. Aubry, J., Passelegue, F.X., Deldicque, D., Girault, F., Marty, S., Lahfid, A., Bhat, H.S., Escartin, J., Schubnel, A.: Frictional heating processes and energy budget during laboratory earthquakes. Geophys. Res. Lett. **45**, 12274–12282 (2018)
7. Bak, P.: How Nature Works: The Science of Self-Organized Criticality. Springer, New York (1996)
8. Ballerini, M., Cabibbo, N., Candelier, R., Cavagna, A., Cisbani, E., Giardina, I., Orlandi, A., Parisi, G., Procaccini, A., Viale, M., Zdravkovic, V.: Empirical investigation of starling flocks: a benchmark study in collective animal behaviour. Anim. Behav. **76**, 201–215 (2008)
9. Billi, A.: Grain size distribution and thickness of breccia and gouge zones from thin (<1m) strike-slip fault cores in limestone. J. Struct. Geol. **27**, 1823–1837 (2005)
10. Bolton, D.C., Marone, C., Saffer, D., Trugman, D.T.: Foreshock properties illuminate nucleation processes of slow and fast laboratory earthquakes. Nat. Commun. (2023). https://doi.org/10.1038/s41467-023-39399-0
11. Buijze, L., Guo, Y., Niemeijer, A.R., Ma, S., Spiers, C.J.: Nucleation of stick-slip instability within a large-scale experimental fault: effects of stress heterogeneities due to loading and gouge layer compaction. J. Geophys. Res. Solid Earth (2020). https://doi.org/10.1029/2019JB018429
12. Buijze, L., Guo, Y., Niemeijer, A.R., Ma, S., Spiers, C.J.: Effects of heterogeneous gouge segments on the slip behavior of experimental faults at dm scale. Earth Planet. Sci. Lett. **554**, 116652 (2021). https://doi.org/10.1016/j.epsl.2020.116652
13. Byerlee, J.D., Brace, W.F.: Stick slip stable sliding and earthquakes - effect of rock type pressure strain rate and stiffness. J. Geophys. Res. **73**, 6031–6031 (1968)
14. Cantor, D., Cárdenas-Barrantes, M., Preechawuttipong, I., Renouf, M., Azéma, E.: Compaction model for highly deformable particle assemblies. Phys. Rev. Lett. **124**, 208003 (2020)
15. Cao, Y., Li, J., Kou, B., Xia, C., Li, Z., Chen, R., Xie, H., Xiao, T., Kob, W., Hong, L., Zhang, J., Wang, Y.: Structural and topological nature of plasticity in sheared granular materials. Nat. Commun. **9**, 2911 (2018)
16. Cavagna, A., Cimarelli, A., Giardina, I., Parisi, G., Santagati, R., Stefanini, F., Viale, M.: Scale-free correlations in starling flocks. Proc. Natl. Acad. Sci. U. S. A. **107**, 11865–11870 (2010)
17. Cavagna, A., Giardina, I., Orlandi, A., Parisi, G., Procaccini, A.: The STARFLAG handbook on collective animal behaviour: 2. Three-dimensional analysis. Anim. Behav. **76**, 237–248 (2008)
18. Cavagna, A., Giardina, I., Orlandi, A., Parisi, G., Procaccini, A., Viale, M., Zdravkovic, V.: The STARFLAG handbook on collective animal behaviour: 1. Empirical methods. Anim. Behav. **76**, 217–236 (2008)
19. Chikkadi, V., Schall, P.: Nonaffine measures of particle displacements in sheared colloidal glasses. Phys. Rev. E (2012). https://doi.org/10.1103/PhysRevE.85.031402
20. Cladouhos, T.T.: Shape preferred orientations of survivor grains in fault gouge. J. Struct. Geol. **21**, 419–436 (1999)
21. Cundall, P.A., Strack, O.D.L.: A discrete numerical model for granular assemblies. Geotechnique **29**, 47–65 (1979)
22. Daniels, K.E., Hayman, N.W.: Force chains in seismogenic faults visualized with photoelastic granular shear experiments. J. Geophys. Res. Solid Earth (2008). https://doi.org/10.1029/2008JB005781
23. Dong, P., Wang, Z., Ying, X., Xia, K.: Effects of fault roughness on estimating critical slip-weakening distance from fault slip history: a laboratory study. Tectonophysics **885**, 230419 (2024). https://doi.org/10.1016/j.tecto.2024.230419
24. Dorostkar, O., Guyer, R.A., Johnson, P.A., Marone, C., Carmeliet, J.: Cohesion-induced stabilization in stick-slip dynamics of weakly wet, sheared granular fault gouge. J. Geophys. Res. Solid Earth **123**, 2115–2126 (2018)
25. Engelder, J.T.: Cataclasis and the generation of fault gouge. GSA Bull. **85**, 1515–1522 (1974)
26. Ferdowsi, B., Griffa, M., Guyer, R.A., Johnson, P.A., Marone, C., Carmeliet, J.: Microslips as precursors of large slip events in the stick-slip dynamics of sheared granular layers: a discrete element model analysis. Geophys. Res. Lett. **40**, 4194–4198 (2013)
27. Ferdowsi, B., Griffa, M., Guyer, R.A., Johnson, P.A., Marone, C., Carmeliet, J.: Three-dimensional discrete element modeling of triggered slip in sheared granular media. Phys. Rev. E Stat. Nonlin. Soft Matter Phys. **89**, 042204 (2014)
28. Fournier, T., Morgan, J.: Insights to slip behavior on rough faults using discrete element modeling. Geophys. Res. Lett. (2012). https://doi.org/10.1029/2012GL051899
29. Gao, K., Euser, B.J., Rougier, E., Guyer, R.A., Lei, Z., Knight, E.E., Carmeliet, J., Johnson, P.A.: Modeling of stick-slip behavior in sheared granular fault gouge using the combined finite-discrete element method. J. Geophys. Res. Solid Earth **123**, 5774–5792 (2018)
30. Gao, K., Guyer, R., Rougier, E., Ren, C.X., Johnson, P.A.: From stress chains to acoustic emission. Phys. Rev. Lett. **123**, 048003 (2019)
31. Gao, K., Guyer, R.A., Rougier, E., Johnson, P.A.: Plate motion in sheared granular fault system. Earth Planet. Sci. Lett. **548**, 116481 (2020). https://doi.org/10.1016/j.epsl.2020.116481
32. Geller, D.A., Ecke, R.E., Dahmen, K.A., Backhaus, S.: Stick-slip behavior in a continuum-granular experiment. Phys. Rev. E Stat. Nonlinear Soft Matter Phys. **92**, 060201 (2015)
33. Goebel, T.H.W., Schuster, V., Kwiatek, G., Pandey, K., Dresen, G.: A laboratory perspective on accelerating preparatory processes before earthquakes and implications for foreshock detectability. Nat. Commun. (2024). https://doi.org/10.1038/s41467-024-49959-7
34. Gridin, G.A., Kocharyan, G.G., Morozova, K.G., Novikova, E.V., Ostapchuk, A.A., Pavlov, D.V.: Evolution of sliding along a heterogeneous fault. A large-scale laboratory experiment. Izvestiya-Phys. Solid Earth **59**, 460–467 (2023)
35. Ikari, M.J., Ito, Y., Ujiie, K., Kopf, A.J.: Spectrum of slip behaviour in Tohoku fault zone samples at plate tectonic slip rates. Nat. Geosci. **8**, 870–874 (2015)
36. Ikari, M.J., Marone, C., Saffer, D.M.: On the relation between fault strength and frictional stability. Geology **39**, 83–86 (2011)
37. Lherminier, S., Planet, R., Vehel, V.L.D., Simon, G., Vanel, L., Måløy, K.J., Ramos, O.: Continuously sheared granular matter

reproduces in detail seismicity laws. Phys. Rev. Lett. **122**, 218501 (2019)
38. Mair, K., Abe, S.: 3D numerical simulations of fault gouge evolution during shear: grain size reduction and strain localization. Earth Planet. Sci. Lett. **274**, 72–81 (2008)
39. Mair, K., Hazzard, J.F.: Nature of stress accommodation in sheared granular material: Insights from 3D numerical modeling. Earth Planet. Sci. Lett. **259**, 469–485 (2007)
40. Marone, C.: The effect of loading rate on static friction and the rate of fault healing during the earthquake cycle. Nature **391**, 69–72 (1998)
41. Marone, C.: Laboratory-derived friction laws and their application to seismic faulting. Annu. Rev. Earth Planet. Sci. **26**, 643–696 (1998)
42. Matochkina, S.D., Shebalin, P.N., Smirnov, V.B., Ponomarev, A.V., Malyutin, P.A.: Acoustic emission events clustering parameters in laboratory rock fracture experiments. Izvestiya-Phys. Solid Earth **60**, 913–922 (2024)
43. McLaskey, G.C.: Earthquake initiation from laboratory observations and implications for foreshocks. J. Geophys. Res. Solid Earth **124**, 12882–12904 (2019)
44. Mehta, A.: Granular Physics. Cambridge University Press, Cambridge (2007)
45. Mollon, G., Aubry, J., Schubnel, A.: Simulating melting in 2D seismic fault gouge. J. Geophys. Res. Solid Earth **126**, e2020JB021485 (2021)
46. Mollon, G., Aubry, J., Schubnel, A.: Laboratory earthquakes simulations—typical events, fault damage, and gouge production. J. Geophys. Res. Solid Earth **128**, e2022JB025429 (2023)
47. Mollon, G., Aubry, J., Schubnel, A.: Laboratory earthquakes simulations—emergence, structure, and evolution of fault heterogeneity. J. Geophys. Res. Solid Earth **129**, 28626 (2024)
48. Munjiza, A.: The Combined Finite-Discrete Element Method. Wiley, London (2004)
49. O'Sullivan, C.: Particulate Discrete Element Modelling: A Geomechanics Perspective. CRC Press, Florida (2011)
50. Oda, M., Iwashita, K.: Mechanics of Granular Materials: An Introduction. CRC Press, Florida (1990)
51. Okubo, A.: Dynamical aspects of animal grouping: swarms, schools, flocks, and herds. Adv. Biophys. **22**, 1–94 (1986)
52. Passelegue, F.X., Aubry, J., Nicolas, A., Fondriest, M., Deldicque, D., Schubnel, A., Di Toro, G.: From fault creep to slow and fast earthquakes in carbonates. Geology **47**, 744–748 (2019)
53. Power, W.L., Tullis, T.E., Brown, S.R., Boitnott, G.N., Scholz, C.H.: Roughness of natural fault surfaces. Geophys. Res. Lett. **14**, 29–32 (1987)
54. Pozzi, G., De Paola, N., Nielsen, S.B., Holdsworth, R.E., Tesei, T., Thieme, M., Demouchy, S.: Coseismic fault lubrication by viscous deformation. Nat. Geosci. **14**, 437–442 (2021)
55. Rubino, V., Lapusta, N., Rosakis, A.J.: Intermittent lab earthquakes in dynamically weakening fault gouge. Nature **606**, 922–929 (2022)
56. Sammis, C., King, G., Biegel, R.: The kinematics of gouge deformation. Pure Appl. Geophys. **125**, 777–812 (1987)
57. Scuderi, M.M., Collettini, C., Viti, C., Tinti, E., Marone, C.: Evolution of shear fabric in granular fault gouge from stable sliding to stick slip and implications for fault slip mode. Geology (2017). https://doi.org/10.1130/G39033.1
58. Song, J.Y., McLaskey, G.C.: Laboratory earthquake ruptures contained by velocity strengthening fault patches. J. Geophys. Res. Solid Earth (2024). https://doi.org/10.1029/2023JB028509
59. Tal, Y., Faulkner, D.: The effect of fault roughness and earthquake ruptures on the evolution and scaling of fault damage zones. J. Geophys. Res. Solid Earth (2022). https://doi.org/10.1029/2021JB023352
60. Thieme, M., Pozzi, G., Demouchy, S., De Paola, N., Barou, F., Koizumi, S., Bowen, L.: Shear deformation of nano- and microcrystalline olivine at seismic slip rates. Tectonophysics **802**, 228736 (2021)
61. Tsai, J.-C., Voth, G.A., Gollub, J.P.: Internal granular dynamics, shear-induced crystallization, and compaction steps. Phys. Rev. Lett. (2003). https://doi.org/10.1103/PhysRevLett.91.064301
62. Wang, C., Elsworth, D., Fang, Y.: Ensemble shear strength, stability, and permeability of mixed mineralogy fault gouge recovered from 3D granular models. J. Geophys. Res. Solid Earth **124**, 425–441 (2019)
63. Xia, K., Rosakis, A.J.: Laboratory earthquakes along faults with a low velocity zone: Directionality and pulse-like ruptures. Extreme Mech. Lett. **46**, 101321 (2021). https://doi.org/10.1016/j.eml.2021.101321
64. Xing, Y., Zheng, J., Li, J., Cao, Y., Pan, W., Zhang, J., Wang, Y.: X-ray tomography investigation of cyclically sheared granular materials. Phys. Rev. Lett. **126**, 048002 (2021)
65. Xu, S., Fukuyama, E., Yamashita, F., Kawakata, H., Mizoguchi, K., Takizawa, S.: Fault strength and rupture process controlled by fault surface topography. Nat. Geosci. **16**, 94–100 (2023)
66. Yamashita, F., Fukuyama, E., Xu, S.Q., Mizoguchi, K., Kawakata, H., Takizawa, S.: Rupture preparation process controlled by surface roughness on meter-scale laboratory fault. Tectonophysics **733**, 193–208 (2018)
67. Zhang, Y., Gao, K., Li, C.: Two slip regimes in sheared granular fault. Earth Planet. Sci. Lett. **608**, 118086 (2023). https://doi.org/10.1016/j.epsl.2023.118086
68. Zhao, Y., Zhao, Y., Wang, D., Zheng, H., Chakraborty, B., Socolar, J.E.S.: Ultrastable shear-jammed granular material. Phys. Rev. X (2022). https://doi.org/10.1103/PhysRevX.12.031021
69. Zou, Y., Ma, G., Mei, J., Zhao, J., Zhou, W.: Microscopic origin of shape-dependent shear strength of granular materials: a granular dynamics perspective. Acta Geotech. **17**, 2697–2710 (2021)